Analytic Expressions of the Transmission, Reflection, and Source Function for the Community Radiative Transfer Model

Quanhua (Mark) Liu[1] and Changyong Cao[1]

[1]Center for Satellite Applications and Research, National Environmental Satellite, Data, and Information Service, NOAA
5830 University Research Court, College Park, MD, USA 20740-3822
Email: quanhua.liu@noaa.gov; phone: (301)-683-3661

AUGUST 24, 2018

Keywords: Vectorized Radiative Transfer, Community Radiative Transfer Model

ABSTRACT

The phase matrix in scalar radiative transfer is symmetric that grants reciprocity principle in radiative transfer. The reciprocity principle is so useful that one may compute a single transmission matrix and a single reflection matrix for a homogeneous medium regardless of in upward or downward direction. The symmetric phase matrix is also important as one only needs to solve for a real eigensolution. An eigensolution is often used in a radiative transfer solver because of its high computational efficiency. However, the phase matrix in vectorized radiative transfer is generally not symmetric which challenges the reciprocity principle and forces us to deal with a complex eigensolution that requires a major effort in computational coding tangent-linear and adjoint models. This paper introduces an approach to retain the reciprocity principle in radiative transfer and applies a Taylor expansion of analytic transmittance and reflection matrices for a base optical depth together with a doubling-adding method beyond the base in the vectorized Community Radiative Transfer Model (CRTM). The value of the base optical depth depends on the maximum absolute value of the phase matrix elements. In comparison with other forward radiative transfer models, the extended vectorized CRTM agrees well with those models. The computational efficiency among the CRTM and those models is comparable. The tangent-linear and adjoint modules of the vectorized CRTM can be used for assimilating microwave, infrared, visible and ultraviolet sensor radiances.

1. INTRODUCTION

A computationally efficient and accurate radiative transfer (RT) model is needed in radiance assimilation for supporting weather forecasting, physical retrievals for satellite environmental data records, and verification and inter-comparison among remote sensing instruments. There are many

components needed by radiative transfer models: gaseous absorptions, molecular, aerosol and cloud scattering, and surface emission and reflection as well as radiative transfer solvers. In this paper, we focus on radiative transfer solvers. A treatise on radiative transfer theory is given in the book by Chandrasekhar [1]. Radiative transfer theory has been widely applied for studying the Earth's atmosphere from space [2][3]. Radiative transfer theory provides the physical foundation for understanding the radiation budget at the Earth's surface and at the top of the atmosphere, climate change, and radiative cooling and heating rates of the atmosphere. Many radiative transfer solvers have been developed [4][5][6]. Some standard computational procedures are described in the book [2][7].

The matrix operator method (MOM) [8] is one of early accurate models in FORTRAN for radiative transfer. The doubling-adding (DA) method [9][10] was developed many years ago, but is still very valuable and accurate. We use the DA method as a reference model in developing our community radiative transfer models. VLIDORT [11] was developed as a vectorized radiative transfer code for forward model and retrieval studies in multiple scattering media. Matrix formulations of radiative transfer including the polarization effect in a coupled atmosphere-ocean system has been published [12]. Recently, Efremenko et al. [13] have reviewed the matrix-exponential formalism in radiative transfer. During the process of developing the community radiative transfer model, a polarized Delta-4-stream model for thermal and microwave radiative transfer has been studied by Liou et al. [14] at the University of California at Los Angeles. The successive order of interaction (SOI) radiative transfer model was developed by Heidinger et al. [15] at the University of Wisconsin.

The SOI algorithm enhances the computational efficiency of successive order of scatterings [16]. Direct ordinate tangent linear radiative transfer (DOTLRT) has been developed by Voronovich et al.

[17]. A simplified vector discrete-ordinate radiative transfer method has been developed by Weng and Liu [18]. We have also developed the advanced doubling-adding method (ADA) [19] and advanced matrix operator method (AMOM) [20]. All radiative transfer codes above are very accurate and valuable. The decision to use which model for satellite radiance assimilation is more about heritage, maintenance, consistency among forward and tangent-linear as well as adjoint models, and further development. In radiance assimilation, tangent-linear and adjoint models are needed [21]. Coding standards within the organization can play an important role as well.

The Community Radiative Transfer Model (CRTM) was developed for un-polarized scattering atmosphere. The polarization calculation in the CRTM currently comes from polarized surface emissivity and reflectivity. However, un-polarized natural light can be polarized by scattering from molecules, aerosols and clouds, and by the reflection and scattering from surfaces [22]. The polarization of light in the atmosphere-surface system contains important signals that have led to major scientific breakthroughs that could not have been achieved by only studying scalar radiance [23][24][25]. The polarization measured by microwave sensors provides unique information to calculate the sea surface wind speed [26], sea surface wind vector [27], and sea ice [28]. The French satellite-based POLarization and Directionality of the Earth Reflectance (POLDER) instrument has been used to obtain the particle shape of ice clouds [29].

Like Radiative Transfer for TIROS Operational Vertical Sounder (RTTOV), CRTM is operationally used in radiance assimilation in supporting daily weather forecasting at numerical prediction centers. Both RTTOV and CRTM are required to have forward, tangent-linear, adjoint, and K-matrix or jacobian models. Radiance tangent linear model provides a computationally efficient way to calculate radiance increments (a vector of the number (N) of sensor channels) for given control

variables with their perturbations. The adjoint model is a very efficient tool to compute the gradient of the cost function. In radiance assimilation, the cost function measures the departure of control variables from background (e.g. 6h forecasting) and the difference between observed radiances and simulated radiances by using the control variables. The gradient of the cost function with respect to the control variable (initial condition) is obtained by a backward integration of the adjoint model. Adjoint radiative transfer model outputs integrated radiance sensitivities (a vector of the number (M) of control variables) on control variables while K-matrix or jacobian outputs channel-dependent radiance sensitivities (a matrix of M x N) on control variables. ECMWF uses adjoint model and tangent-linear model in four-dimensional radiance assimilation. For retrieval algorithms, one-dimensional variation method and jacobian radiances are often used since the memory usage for a single profile is not a big deal.

Recently, radiance assimilation has moved forward to cloudy radiance assimilation. Under precipitation, neglecting polarization effects from rain drops may result in an error of several Kelvins for the polarized brightness temperatures [30]. The CRTM is also requested to assimilate ultraviolet radiation measured by total ozone mapper and nadir profiler. It demands significant effort to write the tangent-linear and adjoint modules for a forward model. This is a major motivation for us to extend the current CRTM to a vectorized radiative transfer, because current CRTM is operational and has forward, tangent-linear, adjoint, and K-matrix or jacobian modules. We first extend the CRTM ADA for vectorized forward, tangent-linear, adjoint, and K-matrix or jacobian radiative transfer calculations since the extension requires small effort, basically changing the array size. In our previous studies, we noticed that CRTM AMOM has better computational efficiency than CRTM ADA. However, the real eigensolution in CRTM AMOM has to be changed to the complex eigensolution for the vectorized radiative transfer in general. This would require

substantially effort in writing tangent-linear and adjoint modules. Therefore, we use a compromised approach here: a Taylor expansion of analytic solutions in CRTM AMOM for a base optical depth and together with a doubling-adding method beyond the base in the CRTM vectorized radiative transfer. This avoids using the complex eigensolution and adds an alternative way in the radiative transfer family.

In the following sections, we will introduce the CRTM model and discuss the radiative transfer solvers. We have set up benchmark numerical experiments and compared the results using DA, VLIDORT, extended CRTM ADA and CRTM AMOM algorithms here.

2. COMMUNITY RADIATIVE TRANSFER MODEL

The Community Radiative Transfer Model (CRTM) is a sensor-based radiative transfer model. It supports more than 100 sensors including sensors on most meteorological satellites and some from other remote sensing satellites. The CRTM is composed of four important modules for gaseous transmittance, surface emission and reflection, cloud and aerosol absorption and scatterings, and solvers for radiative transfer. The CRTM was designed to meet Numerical Weather Prediction (NWP) and other users' needs. Many options are available for users to choose: input surface emissivity; select a subset of channels for a given sensor; turn off scattering calculations; compute radiance at aircraft altitudes; compute aerosol optical depth only; and threading of the CRTM. Figure 1 shows the interface diagram for users (public interface) and internal modules for developers contained in the lower dashed box. The CRTM forward model is used to simulate from satellite measured radiance, which can be used to verify measurement accuracy, uncertainty, and long-term

stability. The K-matrix module is used to compute Jacobian values (i.e. radiance derivative to geophysical parameters), which is used for the inversion processing in retrieval and radiance assimilations. Tangent-linear and adjoint modules are also often applied to radiance assimilation.

The CRTM is a FORTRAN library for users to link to their own code, instead of a graphic user interface. At the CRTM initialization, user selects the sensor/sensors and surface emissivity/reflectance look-up tables. Developers may incorporate their own expertise into the CRTM for any desired applications. The gaseous transmittance describes atmospheric gaseous absorption, so that one can utilize remote sensing information in data assimilation/retrieval systems for atmospheric temperature, moisture, and trace gases such as CO_2, O_3, N_2O, CO, and CH_4 [31]. The aerosol module is fundamental to acquire aerosol type and concentration for studying air quality. The cloud module contains optical properties of six cloud types, providing radiative forcing information for weather forecasting and climate studies. The CRTM surface model includes surface static and atlas-based emissivity/reflectivity for various surface types. Two radiative transfer solvers have been implemented into the CRTM. The advanced matrix operator method (AMOM) [20] is chosen as a baseline. The successive order of interaction (SOI) radiative transfer [15] developed at the University of Wisconsin, has also been implemented in the CRTM.

3. RADIATIVE TRANSFER EQUATION AND SOLVER

The CRTM is a one-dimensional radiative transfer model [19]. This implies that the atmosphere is assumed to be homogeneous in the horizontal direction, a so called plane-parallel atmosphere. Due to the consideration of computational burden and memory usage 15 years ago, scalar radiative transfer solvers were implemented in the CRTM**,** although the CRTM interface has been designed

for both scalar and vectorized radiative transfer solvers. The scalar radiative transfer model is an approximation [32]. In visible and ultraviolet spectra, radiative transfer calculations that utilize the scalar approximation produce intensity errors as large as 10% [33][34]. The scalar approximation may be used for infrared radiative transfer calculations and microwave radiative transfer calculations without precipitations.

We will briefly discuss the current CRTM default solver the advanced matrix operator method (AMOM). Since the doubling-adding part is used in the CRTM solver SOI, we extended both the doubling-adding method (ADA) and analytic matrix operator method (AMOM) to vectorized radiative transfer solvers.

3.1 Scalar radiative transfer

For the plane-parallel atmosphere, a scalar radiance I at a given wavelength can be written as [19]:

$$\mu \frac{dI(\tau,\Omega)}{d\tau} = I(\ ,\ \ ) - \frac{\varpi}{4\pi}\int P(\ ,\ ,\ \ ')I(\ ,\ \ ')d\ \ ' - S(\ ,\ ,\ _0)\ , \quad (1)$$

where the source function is:

$$S(\ ,\mu,\phi,\mu_0,\phi_0) = (1-\varpi)B(T) + \frac{\varpi F}{4\pi}P(\ ,\mu,\phi,-\mu_0,\phi_0)e^{-\frac{\tau}{\mu}}\ . \quad (2)$$

Here μ the cosine of the viewing zenith angle; ϕ the viewing azimuthal angle; μ_0 the cosine of Sun zenith angle and ϕ_0 the Sun azimuthal angle; ϖ the single scattering albedo; the optical depth; $B(T)$the Planck function at a temperature T; F_0 the solar irradiance; P the phase function; and I the radiance. Positive μ and - μ represent upward and downward directions, respectively.

The first term on the right side of Eq.(2) is isotropic thermal emission, which means only the zeroth order Fourier component has a non-zero value. The second term on the right side of Eq.(2) is diffuse

solar radiation. One may remove this diffuse solar radiation by adding direct incoming solar radiation at the top of the atmosphere as a boundary condition [31]. There are various ways to solve the radiative transfer equation, depending on specific applications. One of the ways is to decouple the azimuth angle from the zenith angle by the expansion of the scalar radiance and the phase function as a series of cosine function of the azimuth angle, These are:

$$P(\ ,\mu,\phi,\ \mu',\phi') = \sum_{m=0}^{N-1} \frac{P_m(\tau,\mu,\mu')}{1+\delta_{\ m}} cosm(\phi'-\phi) \quad (3a)$$

$$I(\ ,\mu,\phi) = \sum_{m=0}^{N-1} I_m(\ ,\mu) cos\ m(\phi_0-\phi) \quad (3b)$$

Inserting Eqs.(3a,b) into Eq.(1) and using a discrete ordinate method for the zenith angle, we obtain *N* independent equations on Fourier components.

$$\mu_i \frac{d}{d\tau}\begin{bmatrix} I_m(\ ,\mu_i) \\ -I_m(\ ,-\mu_i)\end{bmatrix} = \begin{bmatrix} I_m(\ ,\mu_i) \\ I_m(\ ,-\mu_i)\end{bmatrix} - \varpi \sum_{j=1}^{N} \begin{bmatrix} P_m(\ ,\mu_i,\mu_j) & P_m(\ ,\mu_i,-\mu_j) \\ P_m(\ ,-\mu_i,\mu_j) & P_m(\ ,-\mu_i,-\mu_j)\end{bmatrix}\begin{bmatrix} I_m(\ ,\mu_j) \\ I_m(\ ,-\mu_j)\end{bmatrix} w_j - \begin{bmatrix} S_m(\ ,\mu_i,-\mu_0) \\ S_m(\ ,-\mu_i,-\mu_0)\end{bmatrix} \quad (4)$$

Where $\mu_i\ and\ w_i$ are Gaussian quadrature points and weights for the zenith angles. For simplicity, we omit the subscript *m* unless otherwise specified.

For the scalar and the first two components of the Stokes vector, we know from the reciprocity principle of radiative transfer [4][6][33][35]:

$$P(\mu_i,\mu_j) = P(-\mu_i,-\mu_j) \quad (5a)$$

and

$$P(\mu_i,-\mu_j) = P(-\mu_i,\mu_j) \quad (5b)$$

Then the 2 by 2 phase matrix is symmetric and Eq.(4) may be simplified as:

$$\mu_i \frac{d}{d\tau}\begin{bmatrix} I_m(\ ,\mu_i) \\ -I_m(\ ,-\mu_i)\end{bmatrix} = \begin{bmatrix} I_m(\ ,\mu_i) \\ I_m(\ ,-\mu_i)\end{bmatrix} - \varpi \sum_{j=1}^{N} \begin{bmatrix} P_m(\ ,\mu_i,\mu_j) & P_m(\ ,\mu_i,-\mu_j) \\ P_m(\ ,\mu_i,-\mu_j) & P_m(\ ,\mu_i,\mu_j)\end{bmatrix}\begin{bmatrix} I_m(\ ,\mu_j) \\ I_m(\ ,-\mu_j)\end{bmatrix} w_j - \begin{bmatrix} S_m(\ ,\mu_i,-\mu_0) \\ S_m(\ ,-\mu_i,-\mu_0)\end{bmatrix} \quad (5c)$$

By arranging Gaussian quadrature points, Eq.(5c) for each Fourier component in upward and downward directions can be written in a matrix-vector form as (The subscripts u (d) indicate upward (downward) directions, respectively):

$$\frac{d}{d\tau}\begin{bmatrix} \boldsymbol{I}_u \\ \boldsymbol{I}_d\end{bmatrix} = -\boldsymbol{A}\begin{bmatrix} \boldsymbol{I}_u \\ \boldsymbol{I}_d\end{bmatrix} - (1-\varpi)B(T)\begin{bmatrix} \boldsymbol{u}^{-1}\boldsymbol{\Xi} \\ -\boldsymbol{u}^{-1}\boldsymbol{\Xi}\end{bmatrix}\delta_{0m} - \frac{\varpi F}{\pi} e^{-\frac{\tau}{\mu}}\begin{bmatrix} \boldsymbol{u}^{-1}\boldsymbol{\phi_u} \\ -\boldsymbol{u}^{-1}\boldsymbol{\phi_d}\end{bmatrix}, \quad (6a)$$

and

$$\boldsymbol{A} = \begin{bmatrix} \boldsymbol{A_{11}} & \boldsymbol{A_{12}} \\ -\boldsymbol{A_{21}} & -\boldsymbol{A_{22}}\end{bmatrix} \quad (6b)$$

$\boldsymbol{\Xi}$ is a vector of N elements with the value of 1. Using Eqs.(5a-b) for the scalar radiative transfer, we can let

$$\boldsymbol{A_{11}} = \boldsymbol{A_{22}} = \boldsymbol{\alpha} \qquad (7a)$$

$$\boldsymbol{A_{12}} = \boldsymbol{A_{21}} = \boldsymbol{\beta} \qquad (7b)$$

The sub-matrices $\boldsymbol{A_{11}}, \boldsymbol{A_{12}}, \boldsymbol{A_{21}}, \boldsymbol{A_{22}}$, are symmetric and we can rewrite Eq.(6b) as

$$\boldsymbol{A} = \begin{bmatrix} \boldsymbol{\alpha} & \boldsymbol{\beta} \\ -\boldsymbol{\beta} & -\boldsymbol{\alpha}\end{bmatrix} \qquad (7c)$$

$\boldsymbol{\alpha}$ and $\boldsymbol{\beta}$ are *N x N* matrices and their elements are given by:

$$\alpha(\mu_i,\mu_j) = [\varpi P(\mu_i,\mu_j)P(\mu_i,\mu_j)w_j - \delta_{ij}]/\mu_i \qquad (7d)$$

$$\beta(\mu_i,-\mu_j) = \varpi P(\mu_i,-\mu_j)w_j/\mu_i \qquad (7e)$$

$\boldsymbol{\phi_u}$ and $\boldsymbol{\phi_d}$ are vectors with the elements $\phi_u(\mu_i) = P(\mu_i,-\mu_0)$ and $\phi_d(-\mu_i) = P(-\mu_i,-\mu_0)$.

δ_{ij} is the Kronecker delta. $\boldsymbol{u}$ is a diagonal matrix with diagonal elements $\boldsymbol{u} = [\mu_1, \mu_2, \ldots\ldots, \mu_N]$. In order to get the solution at a specific zenith angle, one can add cosine of a given zenith angle (e.g. satellite zenith angle) with zero weight to the Gaussian quadrature form above [10]. The solution at a given zenith angle will just be an element within the homogeneous solution, similar to the post processing in DISORT [36].

Eqs.(6a,b) imply the reciprocity principle of radiative transfer and the transmission and reflection at the top are the same as that at the bottom for a homogeneous layer. Eq.(6a) may be solved using the doubling-adding method) [19] or in an eigensystem. Matrix $\boldsymbol{A}$ can be made symmetric and all its eigenvalues and eigenvectors are real. This is important because one can use the ASYMTX (fast) code, otherwise one needs to use a different solution algorithm (e.g. DGEEV from LAPACK Suite [37]) for a general matrix and now has complex eigensolutions. For a given homogeneous layer of optical depth δ and temperature T_1 at the top linearly changing to T_2 at the bottom, we obtain the analytic expressions (see appendix A) for source function vectors in upward and downward directions [38]:

$$\boldsymbol{s}_u = \left[(\boldsymbol{E}-\boldsymbol{t}-\boldsymbol{r})B(T_1) - \big(B(T_2)-B(T_1)\big)\boldsymbol{t} + \frac{B(T_2)-B(T_1)}{(1-\varpi g)\delta}(\boldsymbol{E}+\boldsymbol{r}-\boldsymbol{t})\boldsymbol{u}\right]\boldsymbol{\Xi}\delta_{0m} + e^{-\frac{\tau}{\mu}}\left[\left(\boldsymbol{E} - \boldsymbol{t}e^{-\frac{\delta}{\mu}}\right)\boldsymbol{\Psi}_{\boldsymbol{u}} - \boldsymbol{r}\boldsymbol{\Psi}_{\boldsymbol{d}}\right] \quad (8a)$$

$$\boldsymbol{s}_d = \left[(\boldsymbol{E}-\boldsymbol{t}-\boldsymbol{r})B(T_1) + \big(B(T_2)-B(T_1)\big)(\boldsymbol{E}-\boldsymbol{r}) + \frac{B(T_2)-B(T_1)}{(1-\varpi g)\delta}(\boldsymbol{t}-\boldsymbol{E}-\boldsymbol{r})\boldsymbol{u}\right]\boldsymbol{\Xi}\delta_{0m} + e^{-\frac{\tau}{\mu}}\left[\left(e^{-\frac{\delta}{\mu}}\boldsymbol{E} - \boldsymbol{t}\right)\boldsymbol{\Psi}_{\boldsymbol{d}} - \boldsymbol{r}e^{-\frac{\delta}{\mu}}\boldsymbol{\Psi}_{\boldsymbol{u}}\right] \quad (8b)$$

Where ^{0} the accumulated optical depth above this layer top. In the CRTM, a layer mean temperature is used, instead of level temperatures because NWP model only provides atmospheric layer temperatures. For the case, one can set $B(T_2) = B(T_1) = B(\bar{T})$ in Eqs.(8a-b).

The layer transmittance matrix is,

$$\boldsymbol{t} = 2[\cosh(\boldsymbol{H}\delta) - \boldsymbol{V}sinh(\boldsymbol{H}\delta) + \cosh(\boldsymbol{F}\delta) - \boldsymbol{U}sinh(\boldsymbol{F}\delta)]^{-1} \qquad (8c)$$

and the layer reflection matrix is,

$$\boldsymbol{r} = \frac{1}{2}[\cosh(\boldsymbol{H}\delta) + \boldsymbol{V}sinh(\boldsymbol{H}\delta) - \cosh(\boldsymbol{F}\delta) - \boldsymbol{U}sinh(\boldsymbol{F}\delta)]\boldsymbol{t} \qquad (8d)$$

with $\cosh(\boldsymbol{H}\delta) = [\boldsymbol{exp}(\boldsymbol{H}\delta) + \exp(-\boldsymbol{H}\delta)]/2$, $\sinh(\boldsymbol{H}\delta) = [\boldsymbol{exp}(\boldsymbol{H}\delta) - \exp(-\boldsymbol{H}\delta)]/2$

and $\boldsymbol{H}^2 = (\boldsymbol{\alpha} - \boldsymbol{\beta})(\boldsymbol{\alpha} + \boldsymbol{\beta})$, $\boldsymbol{F}^2 = (\boldsymbol{\alpha} + \boldsymbol{\beta})(\boldsymbol{\alpha} - \boldsymbol{\beta})$, $\boldsymbol{U} = (\boldsymbol{\alpha} - \boldsymbol{\beta})\boldsymbol{F}^{-1}$, $\boldsymbol{V} = (\boldsymbol{\alpha} + \boldsymbol{\beta})\boldsymbol{H}^{-1}$,

The matrix exponentials can be calculated using either their eigensystems or their Taylor expansions. For the scalar radiative transfer in the current CRTM code, we use the solution of the eigensystem because it is fast for the symmetric phase matrix. Looking at the CRTM code, one can see that it is only necessary to deal with the exponential function as function of negative values (-eigenvalue times optical depth). The exponential function with positive values can be rearranged as the exponential function with negative values in the matrix inversion. Therefore, the expressions in transmission and reflection matrices are numerically very stable and accurate. We also noticed that the eigen-solution demands strict conditions on the phase matrix. It can occasionally be a problem (small negative eigenvalue) if the reconstructed phase matrix after a truncation has very small negative values for radiation intensity. The problem may be solved by setting the very small negative value to zero. The algorithm ADA and the Taylor expansion often can be tolerant with the very small negative values in the reconstructed phase matrix.

For a planetary atmosphere, the atmosphere may be divided into *n* optically homogeneous layers. The optical properties (e.g., extinction coefficient, single scattering albedo, and phase matrix) are the same within each layer although the temperature may linearly vary within. Again, there are various methodologies to integrate homogeneous layers [19]. In this study, the adding method is used for integrating the surface and multiple atmospheric layers. The method was applied to flux calculation using a two-stream approximation [39].

In the following, we briefly describe the adding methodology. We denote $\boldsymbol{R_u}(k)$ (upper case) for integrated reflection matrix and $\boldsymbol{I}_u(k)$ for integrated radiance vector at level k in the upward direction. *k=n* and *k=0* represent the surface level and the top of the atmosphere, respectively. The adding method starts from the surface without an atmosphere. At the surface, $\boldsymbol{R_u}(n)$ is the surface reflection matrix and $\boldsymbol{I}_u(n)$ equals the surface emissivity vector multiplied by the Planck function at the surface temperature and from surface reflected solar radiation. The upward reflection matrix and radiance at the new level can be obtained by adding one layer from the present level:

$$\boldsymbol{R_u}(k-1) = \boldsymbol{r}(k) + \boldsymbol{t}(k)[\boldsymbol{E} - \boldsymbol{R_u}(k)\boldsymbol{r}(k)]^{-1}\boldsymbol{R_u}(k)\boldsymbol{t}(k) \quad (9a)$$

$$\boldsymbol{I}_u(k-1) = \boldsymbol{s}_u(k) + \boldsymbol{t}(k)[\boldsymbol{E} - \boldsymbol{R_u}(k)\boldsymbol{r}(k)]^{-1}[\boldsymbol{R_u}(k)\boldsymbol{s}_d(k) + \boldsymbol{I}_u(k)] \quad (9b)$$

Where lower case $\boldsymbol{t}(k), \boldsymbol{r}(k), \boldsymbol{s}(k)$ are layer transmission matrix, reflection matrix, and source vector (see Eqs.(8a-d). The physical meaning of equation (9) is obvious. The first term on the right side of Eq.(9a) is the reflectance of the layer to be added. The second term on the right side of Eq.(9a) is the reflectance due to the radiation from the new level transmitted to and multiple reflected by the present level and then transmitted back to the new level. The three terms on the right side of Eq.(9b) represent the upward layer source, from the present level reflected layer downward source, and from the present level transmitted upward radiance, respectively. The upward radiance $\boldsymbol{I}_u(0)$ at the top of the atmosphere can be obtained by looping the index from *k=n* to *k=1* and adding

the contribution from cosmic background radiance (Planck function at the temperature of 2.7 Kelvin) vector $\boldsymbol{I}_{sky}$, the total radiance at the top of the atmosphere will be

$$\boldsymbol{I}_u = \boldsymbol{I}_u(0) + \boldsymbol{R_u}(0)\boldsymbol{I}_{sky} \quad (9c)$$

Therefore, Eqs.(8a-d) provide the analytic expression for layer source function vectors, transmittance matrix and reflection matrix. Eqs(9a-c) can integrate all layers and return the upwards scalar radiance at the top of the atmosphere. In the CRTM, the default solver (AMOM) mainly processes matrices (n_Angles by n_Angles) and vectors (n_Angles) manipulation where n_Angles represents the number of discrete angles.

3.2 Vectorized Radiative Transfer

The vectorized radiative transfer equation is the same as the scalar radiative transfer except using the Stokes vector (with 4 components: radiance, polarization difference, the plane of polarization and the ellipticity of the electromagnetic wave) to replace intensity. Single phase function element will be replaced by a 4 by 4 matrix, which may destroy the symmetry used in the scalar radiative transfer. Generally speaking, the reciprocity principle (see Eqs.(5a-b) is no longer valid, which means that the transmittance matrix at the layer top is different from the transmittance at the bottom. This is the same true for the reflection matrix. As noted by Siewert [40], both complex variable and real variable eigensolutions may now be present. Left and right eigenvectors will be used. The eigensolver module ASYMTX [36] [41] cannot be used for a general matrix. The complex-variable eigensolver DGEEV from the LAPACK [37] may be used instead. The analytic expressions for the layer transmittance matrix, reflection matrix, and source vectors are no longer valid either. This would require substantial change to the CRTM code. Fortunately, we found that the phase function (scalar) symmetry Eq.(5a-b) can be retained for the phase matrix (vectorized) by just changing the

sign for the third and the fourth Stokes components in the downward direction as Spurr [11] did. Using bold letters for matrices and vectors, Eq.(1) can be rewritten for the vectorized radiative transfer in the case of a macroscopically isotropic and mirror-symmetric medium [42]:

$$\mu \frac{d\boldsymbol{I}(\tau,\mu,\phi)}{d\tau} = \boldsymbol{I}(\ ,\mu,\phi) - \frac{\varpi}{4\pi}\int_0^{2\pi}\int_{-1}^{1}\boldsymbol{P}(\ ,\mu,\phi,\ \mu',\phi')\boldsymbol{I}(\ ,\ \mu',\phi')\mu' d\mu' d\phi' - \boldsymbol{S}(\ ,\mu,\phi,-\mu_0,\phi_0)$$

(10a)

where

$$\boldsymbol{S}(\ ,\mu,\phi,\mu_0,\phi_0) = (1-\varpi)B(T)\begin{bmatrix}1\\0\\0\\0\end{bmatrix} + \frac{\varpi F}{4\pi}\begin{bmatrix}P_{11}(\ ,\mu,\phi,-\mu_0,\phi_0)\\P_{12}(\ ,\mu,\phi,-\mu_0,\phi_0)\\P_{13}(\ ,\mu,\phi,-\mu_0,\phi_0)\\P_{14}(\ ,\mu,\phi,-\mu_0,\phi_0)\end{bmatrix} e^{-\frac{\lambda\tau}{\mu}} \qquad (10b)$$

and

$$\boldsymbol{P} = \boldsymbol{L}(\boldsymbol{\pi}-\boldsymbol{i_2})\begin{bmatrix}F_{11}(\Theta) & F_{12}(\Theta) & 0 & 0\\ F_{12}(\Theta) & F_{22}(\Theta) & 0 & 0\\ 0 & 0 & F_{33}(\Theta) & F_{43}(\Theta)\\ 0 & 0 & -F_{43}(\Theta) & F_{44}(\Theta)\end{bmatrix}\boldsymbol{L}(-\boldsymbol{i_1}) \qquad (10c)$$

P is the phase matrix, a product between the scattering matrix $\boldsymbol{F}(\Theta)$ and rotation matrices $\boldsymbol{L}$. The rotation angle $\boldsymbol{i_1}$ $(\boldsymbol{i_2})$ is the angle between scattering plane and the meridional plane containing the incoming ray (outgoing ray). For spherical particles, we can have $F_{11} = F_{22}$ and $F_{33} = F_{44}$. In radiative transfer calculations, incoming radiation needs to be transformed from the meridian plane to the scattering plane. After computing scattering term, radiation needs to be transformed back to the meridional plane again. The meridional plane contains z-axis and the direction of electromagnetic wave. The scattering plane is composed of incoming and outgoing vectors. Electric field vector of horizontally polarized radiation is normal to the meridian plan while the vertically polarized radiation is parallel to the plane.

The Stokes vector may be expressed as

$$\boldsymbol{I} = [I, Q, U, V]^T = \left[\frac{\langle|E_v|^2+|E_h|^2\rangle}{2}, \frac{\langle|E_v|^2-|E_h|^2\rangle}{2}, 2Re\langle E_v E_h^*\rangle, 2Im\langle E_v E_h^*\rangle\right]^T.$$

E_v and E_h are the vertically (in the meridian plan) and horizontally (perpendicular to the meridian plan) polarized components of electric fields. The angle brackets denote the ensemble average and the asterisk denotes the complex conjugate. Applying the reflector operator, the vertically polarized component remains the same while the horizontally polarized component changes a sign when the sign of the azimuthal angle is changed [43][44][45]. Therefore, the first two components are even function and the third and the fourth components odd function.

There are two boundary conditions needed for the radiative transfer solution. The downward radiation at the top is just cosmic background radiation while solar incoming radiation can be treated as diffuse radiation by the atmosphere and surface. That is

$$\boldsymbol{I}(0, -\mu, \phi) = B(T = 2.73\ \ ) \begin{bmatrix}1\\0\\0\\0\end{bmatrix} \tag{11a}$$

At the surface,

$$\boldsymbol{I}(\ _S, \mu, \phi) = \epsilon(\mu) B(T_S) \begin{bmatrix}1\\0\\0\\0\end{bmatrix} + \frac{\varpi}{4\pi}\int_0^{2\pi}\int_0^1 \boldsymbol{r}(\mu, \phi, -\mu', \phi')\boldsymbol{I}(\ _S, -\mu', \phi')\mu' d\mu' d\phi' +$$

$$\boldsymbol{r}(\mu, \phi, -\mu_0, \phi_0)\frac{\varpi F}{4\pi} e^{-\frac{\lambda\tau_S}{\mu}} \tag{11b}$$

where λ is a geometrical factor for pseudo-spherical beam attenuation. The azimuth and zenith angles are generally coupled. The azimuthal dependence can be separated by use of the Fourier transformation for azimuthal angles. Since the first two components of the Stokes vector are even functions and the last two components of the Stokes vector are odd functions, The phase matrix, the

source function, and the Stokes vector may be expanded as a series of cosine and sine functions as follows:

$$\boldsymbol{P}(\ ,\mu,\phi,\ \mu',\phi') = \sum_{m=0}^{N} \frac{P_m^c(\tau,\mu,\mu')}{1+\delta_{\ m}} \cos(m(\phi'-\phi)) + P_m^s(\ ,\mu,\mu')\sin(m(\phi'-\phi)) \quad (12a)$$

$$\boldsymbol{I}(\ ,\mu,\phi) = \sum_{m=0}^{N} I_m^c(\ ,\mu)cos\ (m(\phi_0-\phi)) + I_m^s(\ ,\mu)sin\ (m(\phi_0-\phi)) \quad (12b)$$

$$\boldsymbol{S}(\ ,\mu,\phi) = \sum_{m=0}^{N} S_m^c(\ ,\mu)cos\ (m(\phi_0-\phi)) + S_m^s(\ ,\mu)sin\ (m(\phi_0-\phi)) \quad (12c)$$

The Fourier components of the phase matrix have some special properties. For spherical particles or randomly oriented non-spherical particles, the sub-matrix off diagonal has only a non-zero sine part, whereas the sub-matrix diagonal has only a non-zero cosine part [40]. Substituting Eqs.(12a-c) into Eqs.(10a-b) and comparing the cosine and sine terms of equal order for the first two and the last two components of the Stokes vector respectively, we have

$$\mu \frac{d\boldsymbol{I_m}(\tau,\mu)}{d\tau} = \boldsymbol{I_m}(\ ,\mu) -$$
$$\varpi \int_0^1 \boldsymbol{P_m}(\ ,\mu,\mu')\boldsymbol{I_m}(\ ,\mu')d\mu' - \varpi \int_0^1 \boldsymbol{P_m}(\ ,\mu,-\mu')\boldsymbol{I_m}(\ ,-\mu')d\mu' - \boldsymbol{S_m}(\ ,\mu,-\mu_0) \quad (13a)$$

$$-\mu \frac{d\boldsymbol{I_m}(\tau,-\mu)}{d\tau} = \boldsymbol{I_m}(\ ,-\mu) -$$
$$\varpi \int_0^1 \boldsymbol{P_m}(\ ,-\mu,\mu')\boldsymbol{I_m}(\ ,\mu')d\mu' - \varpi \int_0^1 \boldsymbol{P_m}(\ ,-\mu,-\mu')\boldsymbol{I_m}(\ ,-\mu')d\mu' - \boldsymbol{S_m}(\ ,-\mu,-\mu_0) \quad (13b)$$

where $\boldsymbol{I}_m = [I_m^c, Q_m^c, U_m^s, V_m^s]^T$ (superscript c for cosine mode and s for sine mode). The harmonic mode of the phase matrix can also be represented as

$$\boldsymbol{P_m}(\ ,\mu,\mu') = \frac{1}{2\pi}\int_0^{2\pi} [\boldsymbol{E}cosm(\phi-\phi') - \boldsymbol{D}sinm(\phi-\phi')]\boldsymbol{P}(\ ,\mu,\phi,\ \mu',\phi')d\phi' \quad (14a)$$

with the unit matrix $\boldsymbol{E} = diag[1,1,1,1]$ and the diagonal matrix $\boldsymbol{D} = diag[1,1,-1,-1]$. The Fourier component of the phase matrix can be calculated after [40],

$$\boldsymbol{P_m}(\ ,\mu,\mu') = \sum_{m=l}^{N} \boldsymbol{P}_l^m(\mu)\boldsymbol{B}_l(\ )\boldsymbol{P}_l^m(\mu') \quad (14b)$$

where

$$\boldsymbol{P}_l^m(\mu) = \begin{bmatrix} P_l^m(\mu) & 0 & 0 & 0 \\ 0 & R_l^m(\mu) & -T_l^m(\mu) & 0 \\ 0 & -T_l^m(\mu) & R_l^m(\mu) & 0 \\ 0 & 0 & 0 & P_l^m(\mu) \end{bmatrix} \tag{15a}$$

and the "Greek matrix coefficients" are:

$$\boldsymbol{B}_l = \begin{bmatrix} \beta_l & \gamma_l & 0 & 0 \\ \gamma_l & \alpha_l & 0 & 0 \\ 0 & 0 & \zeta_l & -\varepsilon_l \\ 0 & 0 & \varepsilon_l & \delta_l \end{bmatrix} \tag{15b}$$

It is obvious that $\boldsymbol{B}_l$ is no longer symmetric if $\varepsilon_l \neq 0$. Rayleigh scatterings is an exception and symmetric because of $\varepsilon_l = 0$. Noticing the relationship [40],

$$\boldsymbol{P}_l^m(-\mu) = (-1)^{l-m}\boldsymbol{D}\boldsymbol{P}_l^m(\mu)\boldsymbol{D}\,, \tag{16a}$$

we can obtain

$$\boldsymbol{D}\boldsymbol{P}_{\boldsymbol{m}}(\ ,-\mu,\mu') = \boldsymbol{P}_{\boldsymbol{m}}(\ ,\mu,-\mu')\boldsymbol{D}\,, \tag{16b}$$

$$\boldsymbol{P}_{\boldsymbol{m}}(\ ,\mu,\mu') = \boldsymbol{D}\boldsymbol{P}_{\boldsymbol{m}}(\ ,-\mu,-\mu')\boldsymbol{D}\,. \tag{16c}$$

The remaining integration over μ for each Fourier component or harmonic component in Eqs.(13a-b) can be replaced by a discrete sum [38] using Gaussian quadrature points μ_i and corresponding weights w_i.

$$\mu_i \begin{bmatrix} \frac{d\boldsymbol{I}_{\boldsymbol{m}}(\tau,\mu_i)}{d\tau} \\ \frac{-d\boldsymbol{I}_{\boldsymbol{m}}(\tau,-\mu_i)}{d\tau} \end{bmatrix} = \begin{bmatrix} \boldsymbol{I}_{\boldsymbol{m}}(\ ,\mu_i) \\ \boldsymbol{I}_{\boldsymbol{m}}(\ ,-\mu_i) \end{bmatrix} - \varpi \sum_{j=1}^{N} \begin{bmatrix} \boldsymbol{P}_{\boldsymbol{m}}(\ ,\mu_i,\mu_j) & \boldsymbol{P}_{\boldsymbol{m}}(\ ,\mu_i,-\mu_j) \\ \boldsymbol{P}_{\boldsymbol{m}}(\ ,-\mu_i,\mu_j) & \boldsymbol{P}_{\boldsymbol{m}}(\ ,-\mu_i,-\mu_j) \end{bmatrix} \begin{bmatrix} \boldsymbol{I}_{\boldsymbol{m}}(\ ,\mu_j) \\ \boldsymbol{I}_{\boldsymbol{m}}(\ ,-\mu_j) \end{bmatrix} w_j - \begin{bmatrix} \boldsymbol{S}_{\boldsymbol{m}}(\ ,\mu_i,-\mu_0) \\ \boldsymbol{S}_{\boldsymbol{m}}(\ ,-\mu_i,-\mu_0) \end{bmatrix} \tag{17}$$

Eq.(17) can be rewritten in a form that we can apply reciprocity principle as documented in [4][6]. Multiplying the downward radiance vector by the $\boldsymbol{D}$ matrix and using Eqs.(16b-c), Eq.(17) can be rewritten as:

$$\mu_i \begin{bmatrix} \frac{d\boldsymbol{I_m}(\tau,\mu_i)}{d\tau} \\ \frac{-d\boldsymbol{DI_m}(\tau,-\mu_i)}{d\tau} \end{bmatrix} = \begin{bmatrix} \boldsymbol{I_m}(\ ,\mu_i) \\ \boldsymbol{DI_m}(\ ,-\mu_i) \end{bmatrix} -$$

$$\varpi \sum_{j=1}^{N} \begin{bmatrix} \boldsymbol{P_m}(\ ,\mu_i,\mu_j) & \boldsymbol{P_m}(\ ,\mu_i,-\mu_j)\boldsymbol{D} \\ \boldsymbol{P_m}(\ ,\mu_i,-\mu_j)\boldsymbol{D} & \boldsymbol{P_m}(\ ,\mu_i,\mu_j) \end{bmatrix} \begin{bmatrix} \boldsymbol{I_m}(\ ,\mu_j) \\ \boldsymbol{DI_m}(\ ,-\mu_j) \end{bmatrix} w_j - \begin{bmatrix} \boldsymbol{S_m}(\ ,\mu_i,-\mu_0) \\ \boldsymbol{DS_m}(\ ,-\mu_i,-\mu_0) \end{bmatrix} \quad (18)$$

We can now redefine

$$\boldsymbol{I'}_m(\ ,-\mu_i) = \boldsymbol{DI_m}(\ ,-\mu_i) \quad (19a)$$

$$\boldsymbol{P'}_m(\ ,\mu_i,-\mu_j) = \boldsymbol{P_m}(\ ,\mu_i,-\mu_j)\boldsymbol{D} \quad (19b)$$

$$\boldsymbol{S'}_m(\ ,-\mu_i,-\mu_0) = \boldsymbol{DS_m}(\ ,-\mu_i,-\mu_0) \quad (19c)$$

$$\mu_i \begin{bmatrix} \frac{d\boldsymbol{I_m}(\tau,\mu_i)}{d\tau} \\ \frac{-d\boldsymbol{I'}_m(\tau,-\mu_i)}{d\tau} \end{bmatrix} = \begin{bmatrix} \boldsymbol{I_m}(\ ,\mu_i) \\ \boldsymbol{I'}_m(\ ,-\mu_i) \end{bmatrix} - \varpi \sum_{j=1}^{N} \begin{bmatrix} \boldsymbol{P_m}(\ ,\mu_i,\mu_j) & \boldsymbol{P'}_m(\ ,\mu_i,-\mu_j) \\ \boldsymbol{P'}_m(\ ,\mu_i,-\mu_j) & \boldsymbol{P_m}(\ ,\mu_i,\mu_j) \end{bmatrix} \begin{bmatrix} \boldsymbol{I_m}(\ ,\mu_j) \\ \boldsymbol{I'}_m(\ ,-\mu_j) \end{bmatrix} w_j -$$

$$\begin{bmatrix} \boldsymbol{S_m}(\ ,\mu_i,-\mu_0) \\ \boldsymbol{S'}_m(\ ,-\mu_i,-\mu_0) \end{bmatrix} \quad (20)$$

Therefore, Eq.(20) (same form as Eq.(5c)) can be rewritten in the same form as for the scalar radiative transfer (see Eq.(6a) and Eq.(7c)) by increasing number of elements from n_Angles to n_Stokes x n_Angles where n_Stokes represents the number of Stokes components (<= 4). It implies that the reciprocity principle can also be valid for vectorized radiative transfer so that transmission and reflection matrices from the top and from the bottom of a homogeneous layer can be the same. This considerably simplifies code implementation and saves half of the computational time associated with scattering. The adding method of the CRTM ADA [19] can be used for vectorized radiative transfer by increasing the number of elements from n_Angles to n_Stokes x n_Angles.

However, the solution is complicated for the current CRTM AMOM where an eigensolution is used. The phase matrix itself for vectorized radiative transfer is generally not symmetric although the reciprocity principle can be valid. Without the symmetry, the eigenvalues and eigenvectors are complex. One may use the LAPACK solver DGEEV instead of using ASYMTX for a symmetric

phase matrix in the current CRTM AMOM. But, the change from real eigenvalues and eigenvectors to complex eigenvalues and eigenvectors would demand a lot of code changes for the CRTM model in particular for the tangent-linear and adjoint parts. The CRTM doubling-adding algorithm is simple, stable, and accurate but it is about slower than the CRTM AMOM for scalar radiative transfer. For a layer optical depth of 100, we noticed that the doubling-adding algorithm spends more than 80% its iterations (or computation) for the optical depth range from 0 to 0.5 and only less than 20% of its computation time is spent for the optical depth from 0.5 up to 128. Therefore, it can greatly improve the efficiency if we can replace the doubling-adding for the first range of the optical depth from 0 to 0.5 (80% CPU time). We can use a Taylor expansion to calculate the transmission and reflection for the first part of the optical depth (actually product of the optical depth and the maximal absolute value of the phase matrix) to 0.5, then use the doubling-adding algorithm for the remaining part. This approach uses a similar concept to the iterated squaring method for the exponential matrix [46]. The main difference is that our Taylor expansions for transmission and reflection matrices are more complicated than the expansion for exponential matrix and the doubling-adding is also more complicated than the doubling exponential matrix.

The Taylor expansion calculation is stable, fast, and accurate for a small optical depth. The doubling-adding iteration is less than 8 times for optical depth from 0.5 up to 128. The combined Taylor expansion and doubling-adding techniques are computationally efficient and numerically very stable and accurate. The Taylor expansion for the transmission and reflection matrices for Eqs.(8c-d) can be written as

$$\cosh(\boldsymbol{H}\delta) - \boldsymbol{V}sinh(\boldsymbol{H}\delta) + \cosh(\boldsymbol{F}\delta) - \boldsymbol{U}sinh(\boldsymbol{F}\delta) = \sum_{\boldsymbol{0}}^{\boldsymbol{N}} \frac{[(\boldsymbol{\alpha}-\boldsymbol{\beta})(\boldsymbol{\alpha}+\boldsymbol{\beta})]^{\boldsymbol{n}}+[(\boldsymbol{\alpha}+\boldsymbol{\beta})(\boldsymbol{\alpha}-\boldsymbol{\beta})]^{\boldsymbol{n}}}{(\boldsymbol{2n})!}\boldsymbol{\delta}^{\boldsymbol{2n}} - \sum_{\boldsymbol{0}}^{\boldsymbol{N}} \frac{(\boldsymbol{\alpha}+\boldsymbol{\beta})[(\boldsymbol{\alpha}-\boldsymbol{\beta})(\boldsymbol{\alpha}+\boldsymbol{\beta})]^{\boldsymbol{n}}+(\boldsymbol{\alpha}-\boldsymbol{\beta})[(\boldsymbol{\alpha}+\boldsymbol{\beta})(\boldsymbol{\alpha}-\boldsymbol{\beta})]^{\boldsymbol{n}}}{(\boldsymbol{2n+1})!}\boldsymbol{\delta}^{\boldsymbol{2n+1}} \quad (21a)$$

$$\cosh(\boldsymbol{H}\delta) + \boldsymbol{V}sinh(\boldsymbol{H}\delta) - \cosh(\boldsymbol{F}\delta) - \boldsymbol{U}sinh(\boldsymbol{F}\delta) = \sum_{\boldsymbol{0}}^{\boldsymbol{N}} \frac{[(\boldsymbol{\alpha}-\boldsymbol{\beta})(\boldsymbol{\alpha}+\boldsymbol{\beta})]^{\boldsymbol{n}}-[(\boldsymbol{\alpha}+\boldsymbol{\beta})(\boldsymbol{\alpha}-\boldsymbol{\beta})]^{\boldsymbol{n}}}{(\boldsymbol{2n})!}\boldsymbol{\delta}^{\boldsymbol{2n}} +$$

$$\sum_{\boldsymbol{0}}^{\boldsymbol{N}} \frac{(\boldsymbol{\alpha}+\boldsymbol{\beta})[(\boldsymbol{\alpha}-\boldsymbol{\beta})(\boldsymbol{\alpha}+\boldsymbol{\beta})]^{\boldsymbol{n}}+(\boldsymbol{\alpha}-\boldsymbol{\beta})[(\boldsymbol{\alpha}+\boldsymbol{\beta})(\boldsymbol{\alpha}-\boldsymbol{\beta})]^{\boldsymbol{n}}}{(\boldsymbol{2n+1})!}\boldsymbol{\delta}^{\boldsymbol{2n+1}} \quad (21b)$$

Using N = 5 is sufficient for the small value of the first range of the optical depth.

4. PHASE MATRIX

The phase matrix is an important part in radiative transfer. It governs intensity scattering and polarization. Because of polarization, one has to transform the incoming Stokes vector to the scattering plane by multiplying rotation matrices. It requires significant efforts to calculate the phase matrix in particular for non-spherical particles [47]. Fortunately, there are several codes publicly available for calculation the phase matrices [48][49]. We have applied the T-matrix code to compute the phase matrix for dust of spheroids. Invariant imbedding T-matrix method and the separation of variables method have been applied to large non-spherical inhomogeneous particles [50]. Tabulated scattering matrices in generalized spherical functions are also available [51]. As long as one has the data of six elements of scattering matrices, one can use the Legendre expansion coefficients through the integration over azimuth angles [10] for each Fourier component. One can also use Greek matrix coefficients to get around the integration over azimuth angles. In the CRTM, we use the Greek matrix coefficients. For the benchmark experiments in the following section, we choose two phase matrices for: Rayleigh scattering and the scattering in an atmosphere of randomly oriented oblate spheroids with aspect ratio 1.999987, size parameter 3 and index of refraction (1.53,0.006*i*)[52]. Rayleigh scattering is for molecular scattering or for a very small particle in comparison to the electromagnetic wavelength. For example the radius of an oxygen molecule is about 0.2 nanometer (nm), which is much smaller than Ultraviolet (UV) wavelength (sub-micrometer) and microwave

wavelength (millimeter to centimeter) we studied here. For both Rayleigh scattering phase matrix is symmetric. The phase matrix is symmetric if the Greek coefficient $\varepsilon_l = 0$. The second phase function is more generic and widely used in the benchmark experiments [40][11]. Table 1a lists the Legendre expansion coefficients for Rayleigh scattering that will be used in doubling-adding method [10]. Table 1b is the Greek matrix coefficients for Rayleigh scattering that are used in VLIDORT, extended CRTM ADA and AMOM algorithms. The same is true in tables 2a and 2b for the Legendre expansion coefficients and Greek matrix coefficients.

There are few analytic phase functions used in real applications. With specific interest, we discuss three analytic phase functions here. The phase functions are not used for benchmark experiment below. Rayleigh phase function is important for scattering of very small particles. Henyey-Greenstein (HG) phase function can catch up the first moment (e.g. the asymmetry factor g) and can only be used for scalar radiative transfer. The HG phase function may be a good approximation when the asymmetry is a dominant feature. Obviously, HG is only constant for g=0, which cannot represent Rayleigh scattering. We found that combining Rayleigh and HG phase function can work well for some applications. Henyey-Greenstein and Rayleigh (HG-Rayleigh) scattering [53] leads to an analytic function that may be used for a wake asymmetric scattering in microwave range, good for the Mie size parameter smaller or comparable to electromagnetic wavelength.

For polarimetric radiation, the HG-Rayleigh scattering matrix can be written as

$$P(\Theta, g) = \frac{2}{2+G^2}\frac{1-G^2}{(1+G^2-2Gcos(\Theta))^{3/2}}\begin{bmatrix} 1+cos^2\Theta & -1+cos^2\Theta & 0 & 0 \\ -1+cos^2\Theta & 1+cos^2\Theta & 0 & 0 \\ 0 & 0 & cos(\Theta) & 0 \\ 0 & 0 & 0 & cos(\Theta) \end{bmatrix} \quad (22a)$$

where G is called an effective asymmetry factor that can be calculated from the original asymmetry factor g:

$$G = \frac{5}{9}g + \sqrt[3]{\frac{1}{2}\left(\frac{10}{9}g + \frac{250}{729}g^3\right) + \sqrt{\Delta}} - \sqrt[3]{\sqrt{\Delta} - \frac{1}{2}\left(\frac{10}{9}g + \frac{250}{729}g^3\right)} \quad (22b)$$

$$\text{where } \Delta = \left[\frac{1}{2}\left(\frac{10}{9}g + \frac{250}{729}g^3\right)\right]^2 + \left[\frac{1}{3}\left(4 - \frac{25}{27}g^2\right)\right]^3. \quad (22c)$$

Using the effective asymmetry factor, one can recover the original asymmetry factor. Tables 3a and 3b are the Legendre expansion coefficients and Greek matrix coefficients for the phase function at 183 GHz derived for randomly oriented ice crystals with a maximum size of 300 μm and a width of 100 μm [14]. The volume equivalent radius of a sphere is 90 μm and the asymmetry factor equals 0.027. We compare Rayleigh, Henyey-Greenstein, HG-Rayleigh functions with the original phase function. As shown in Figure 2a, the phase element for the intensity (see black line) has larger forward but smaller backward parts in comparison to the Rayleigh scattering (see black dashed line). The original phase function is substantially different from the Henyey-Greenstein phase function for the same asymmetry factor (see red line). This indicates again that HG phase function is not appropriate for weak asymmetry scattering. The HG-Rayleigh phase function (see green line) agrees with the original phase function extremely well. The phase element for linear polarization is given in Figure 2b. The curves of the original, Rayleigh, and HG-Rayleigh phase functions in Figure 2b are almost the same. Using HG-Rayleigh phase function, the calculated brightness temperatures agree well with those using the original phase function [53].

In the CRTM, we actually use the phase function data of non-spherical ice clouds for infrared and UV and visible sensors [54]. We use the formula from [55] to compute the Greek matrix coefficients from the phase function data.

5. BENCHMARK EXPERIMENT

In the benchmark experiments, we use the doubling-adding (DA) method [10], VLIDORT [11], the extended CRTM ADA [19], and the extended CRTM AMOM [20]. The DA method [10] was developed many years ago, but the solution of the method is still very stable and accurate. VLIDORT can compute both radiance and its Jacobian and contains many functions that are very useful for many applications. VLIDORT can be used for full Stokes calculations and achieves very high accuracy. The CRTM ADA [19] was for a scalar radiative transfer. We easily extended the CRTM ADA to fully vectorized radiative transfer by changing the dimension size from n_Angles to n_Angles x n_Stokes, because Eq.(20) satisfies the radiative reciprocity principle. The extension of CRTM ADA works well for both scalar and vectorized radiative transfer. Same did for the CRTM AMOM. But, it works only for the case $\varepsilon_l = 0$ in the Greek matrix coefficients, for example for Rayleigh scattering. For Rayleigh scattering, CRTM ADA is about four times slower than that AMOM using the real eigenvalues and real eigenvectors. For general cases ($\varepsilon_l \neq 0$) where matrix is not symmetric, the extended CRTM AMOM is not applicable. We will use the Taylor expansion (see Eqs.(21a-b) with the doubling-adding algorithm. This method will keep the solver simple, stable, and accurate, and about 2 to 3 times faster than CRTM ADA.

For simplicity, we choose one optically homogeneous layer over a Lambertian surface. The surface albedo is set to 0.25. Solar zenith angle is set to 36.8699 degree (or cosine of the solar zenith angle 0.8) and azimuth angle is set to zero degree. The viewing zenith angle is set to 50.21 degree and the viewing azimuth angle is set to 90 degree. The solar flux is normalized to π. The surface temperature and atmospheric layer temperature are set 300 K. The central wavelength of channel 1 of GOES-16, 470 nm, is used. This configuration is one of the cases of Coulson et al. [56]. DA [10], CRTM ADA

and CRTM AMOM add the viewing zenith angle associated with a zero weight into Gauss quadrature. While VLIDORT applies a post processing step to calculate the solution at the given zenith angle. Both methods are one kind of interpolation for the given zenith angle among solutions at Gaussian quadrature points.

The Rayleigh scattering phase function and the phase function for scattering in an atmosphere of randomly oriented oblate spheroids [52] are used. Rayleigh scattering is for molecular scattering or for a small particle in comparison to electromagnetic wavelength. The Greek matrix coefficients in Eq.(15b) are symmetric for Rayleigh scattering ($\varepsilon_l = 0$). Table 4a is the Rayleigh scattering for an optical depth of 0.1 using four streams. The four streams (two in upward and two in downward directions) should be good for the flux calculation for Rayleigh scatterings that only have three expansion terms for its phase matrix. Table 4b is for the same case but using 16 streams. Same applies to Table 5a and 5b but for an optical depth of 1. As one can see from Tables 4a and 4b that results among all four solvers (DA, VLIDORT, CRTM ADA, and CRTM AMOM) agree well. One may also notice that the relative difference in Q (the second Stokes component) between using four and sixteen streams can be large. This may be due to the fact using the upward solutions from two Gaussian quadrature points is not sufficient in the interpolation for non-linear function Q at the given angle.

The second phase function is more generic and widely used in the benchmark experiment [11][40]. Each element of the phase function has 12 terms or uses 12 expansion coefficients. Results from all the four radiative transfer solvers agree very well for various optical depths. Tables 6, 7, 8, and 9 are for the optical depth of 0.1, 1.0, 10.0, and 100, respectively. All four solvers generate accurate results.

Computational efficiency or speed is certainly important. We realize that such an assessment depends on the applications, computers, computer operation system and compilers. The comparisons we show here are just for simple cases used for tables 6, 7, 8, and 9. For the same algorithm, programming skills may play an important role on the computational efficiency. We use single CPU and GFORTRAN Red Hat 4.8.5-36. Table 10 lists the CPU time difference between calling CPU_Time at the end and the beginning of the RT model code. As one can see that the CPU time usage for VLIDORT is roughly constant for all optical depths. The CPU time for the vectorized CRTM AMOM depends on the optical depth and increases with optical depths. The CPU time between VLIDORT and CRTM AMOM is very close when optical depth increases to 1000.

6. DISCUSSION

In this paper, we discussed the extension of the CRTM solvers ADA and AMOM for vectorized radiative transfer. Generally speaking, Greek matrix coefficients are not symmetric which results in a non-symmetric phase matrix and the vectorized radiative transfer doesn't hold reciprocity principle. Without the reciprocity principle, one has to calculate transmission and reflection matrices at the layer top and bottom separately even for a homogeneous layer. This requires more coding and degrades the computational efficiency. Fortunately, by changing the sign of the third and the fourth Stokes components only in the downward direction as Spurr [11] did, we can get the same form of radiative transfer for both scalar and vectorized radiative transfer, which confirms the reciprocity principle. With the reciprocity principle, we extend the CRTM ADA to vectorized radiative transfer just by changing the dimension size from n_Angles to n_Angles x n_Stokes and save about 50% computational time in the radiative transfer solver part. This also applies to the CRTM AMOM.

However, the extended CRTM AMOM is only applicable to the Greek matrix coefficient $\varepsilon_l = 0$. The extended CRTM AMOM can also be used for the first two components (I and Q or vertically and horizontally polarized brightness temperatures T_v and T_h) that is useful for many microwave radiative transfer applications. For the cases of $\varepsilon_l \neq 0$, we use the combined a Taylor expansion and a doubling-adding method in the CRTM AMOM which are computationally efficient.

We can use a Taylor expansion to calculate the transmission and reflection for an initial optical depth (or base value) (actual product of the optical and the maximal value of the phase matrix), then use the doubling-adding algorithm for the rest part. The base value is small but much larger than the base value (~ 10^{-7})used in ADA. CRTM AMOM requires additional 8 DA iterations for the optical depth less than 128, instead of 34 iterations needed by CRTM ADA. That is why the combined Taylor and DA method is faster than CRTM ADA. Certainly, the doubling-adding algorithm is not required if the optical depth is less than the base value. This method is simple and only requires small effort in coding for radiative transfer forward, tangent linear, adjoint, and K-matrix or jacobian modules. The Taylor expansion convergences fast for a small base value of the optical depth. The computational efficiency may be comparable or somewhat slow to solving a complex eigensystem that can also be used for the CRTM AMOM in the future. We have compared CRTM AMOM using Taylor and DA combination against the solver part of VLIDORT and found that the computational efficiency between the two solvers is comparable.

As discussed in the section of benchmark experiments, all solvers (DA, VLIDORT, CRTM ADA, and CRTM AMOM) are accurate. Extension rather than the implementation of other existing solver is due to considerations of heritage, cost, and maintenance. Another factor is that the analytic

expressions for the transmission, reflection, and source function may be interesting to the community.

One also needs to realize that while the computational capability of radiative transfer calculations increases quickly, the applications demand computational resource much more rapidly. Thirty years ago, the advanced microwave sounder unit (AMSU) on NOAA-15 had a spatial resolution of about 16 km at nadir, a much higher resolution than the gridded resolution of global numerical prediction model. Today, the gridded resolution of a global prediction model is better than that of the current AMSU and Advanced Technology Microwave Sounder (ATMS) at nadir, much better at off-nadir and may demand radiative transfer calculations in three dimensions. For microwave instruments with a spatial resolution of 5 km or better, three-dimensional radiative transfer model needs to be applied to take the radiation leaking from sides into account. It would be a great challenge to use 3D radiative transfer calculations in operations [36]. It requires tremendous work to write tangent-linear and adjoint codes for three-dimensional radiative transfer models. Some software is available online (e.g. http://www-sop.inria.fr/ecuador/tapenade/distrib/1903/taplsnGRgL2/README.html) to translate the forward code to tangent-linear code and adjoint code. We tried to use the software Tapenade to do the conversion for ASYMTX. It did help for the tangent-linear code, but not successful for the adjoint code. The software is still being currently developed. Artificial Intelligence (AI) or deep machine learning could be one of the solutions which is about 1000 times faster than rigorous radiative transfer calculations and the tangent linear and adjoint parts are straightforward.

Acknowledgments

This work was partially supported by Joint Polar Satellite System Proving Ground and Risk Reduction Program. Many thanks to Dr. XingMing Liang for providing the VLIDORT results. We thank Dr. Patrick Stegmann very much for his detailed correction on this paper. The manuscript contents are solely the opinions of the authors and do not constitute a statement of policy, decision, or position on behalf of NOAA or the U.S. government.

Appendix A

This appendix shows how to derive the analytic expressions of layer transmittance matrix, reflection matrix, and source vectors in Eqs.(8a-d). For an atmospheric layer having a top temperature of $T_1(\ ' = 0)$ and a bottom temperature of $T_2(\ ' = \delta)$, we can have (see Eq.(6a)):

$$\frac{d}{d\tau}\begin{bmatrix}\boldsymbol{I}_u\\ \boldsymbol{I}_d\end{bmatrix} = -\boldsymbol{A}\begin{bmatrix}\boldsymbol{I}_u\\ \boldsymbol{I}_d\end{bmatrix} - (1-\varpi)B(T)\begin{bmatrix}\boldsymbol{u}^{-1}\boldsymbol{\Xi}\\ -\boldsymbol{u}^{-1}\boldsymbol{\Xi}\end{bmatrix}\delta_{0m} - \frac{\varpi F}{\pi}e^{-\frac{\tau}{\mu}}\begin{bmatrix}\boldsymbol{u}^{-1}\boldsymbol{\phi_u}\\ -\boldsymbol{u}^{-1}\boldsymbol{\phi_d}\end{bmatrix} \quad \text{(A1)}$$

Where $B(T) = B(T_1) + \frac{B(T_2)-B(T_1)}{\delta}\ ' = b_0 + b_1\ '$ (A2)

Multiplying $e^{\mathbf{A}\tau'}$ on both sides of Eq.(A1) and integrating from zero to the layer optical depth δ, one can have

$$\begin{bmatrix}I_u(\delta)\\ I_d(\delta)\end{bmatrix} = e^{-\mathbf{A}\delta}\begin{bmatrix}I_u(0)\\ I_d(0)\end{bmatrix} - (1-\varpi)\left\{b_1\delta + \left[\begin{bmatrix}\boldsymbol{E} & 0\\ 0 & \boldsymbol{E}\end{bmatrix} - e^{-\mathbf{A}\delta}\right](b_0 - b_1\mathbf{A}^{-1})\right\}\mathbf{A}^{-1}\begin{bmatrix}\boldsymbol{u}^{-1}\boldsymbol{\Xi}\\ -\boldsymbol{u}^{-1}\boldsymbol{\Xi}\end{bmatrix}\delta_{0m} -$$

$$e^{-\frac{\tau}{\mu}}\left\{e^{-\frac{\delta}{\mu}} - e^{-\mathbf{A}\delta}\right\}\begin{bmatrix}\boldsymbol{\Psi_u}\\ \boldsymbol{\Psi_d}\end{bmatrix} \quad \text{(A3)}$$

where $\begin{bmatrix}\boldsymbol{\Psi_u}\\ \boldsymbol{\Psi_d}\end{bmatrix} = -\frac{\varpi F}{\pi}(\boldsymbol{A} - \frac{1}{\mu})^{-1}\begin{bmatrix}\boldsymbol{u}^{-1}\boldsymbol{\phi_u}\\ -\boldsymbol{u}^{-1}\boldsymbol{\phi_d}\end{bmatrix}$ (A4)

and ^{0} the accumulated optical depth above this layer top.

Noticing that thermal emission is isotropic and it only contributes to zeroth Fourier component and the zeroth component of the phase matrix is normalized, one can derive the following relationships for the zeroth component:

$$(1-\omega)\mathbf{A}^{-1}\begin{bmatrix}-\boldsymbol{u}^{-1}\boldsymbol{\Xi}\\ \boldsymbol{u}^{-1}\boldsymbol{\Xi}\end{bmatrix}=\begin{bmatrix}\boldsymbol{\Xi}\\ \boldsymbol{\Xi}\end{bmatrix} \tag{A5}$$

$$(1-\omega)\mathbf{A}^{-2}\begin{bmatrix}-\boldsymbol{u}^{-1}\boldsymbol{\Xi}\\ \boldsymbol{u}^{-1}\boldsymbol{\Xi}\end{bmatrix}=\mathbf{A}^{-1}\begin{bmatrix}\boldsymbol{\Xi}\\ \boldsymbol{\Xi}\end{bmatrix}=\frac{1}{1-\varpi g}\begin{bmatrix}-\boldsymbol{u}\boldsymbol{\Xi}\\ \boldsymbol{u}\boldsymbol{\Xi}\end{bmatrix} \tag{A6}$$

Eq.(A3) can be rewritten as:

$$\begin{bmatrix}I_u(\delta)\\ I_d(\delta)\end{bmatrix}=e^{-\mathbf{A}\delta}\begin{bmatrix}I_u(0)\\ I_d(0)\end{bmatrix}+b_1\delta\begin{bmatrix}\boldsymbol{\Xi}\\ \boldsymbol{\Xi}\end{bmatrix}+\left\{\begin{bmatrix}\boldsymbol{E} & 0\\ 0 & \boldsymbol{E}\end{bmatrix}-e^{-\mathbf{A}\delta}\right\}\left\{b_0\begin{bmatrix}\boldsymbol{\Xi}\\ \boldsymbol{\Xi}\end{bmatrix}-\frac{1}{1-\varpi g}b_1\begin{bmatrix}-\boldsymbol{u}\boldsymbol{\Xi}\\ \boldsymbol{u}\boldsymbol{\Xi}\end{bmatrix}\right\}$$

$$-e^{-\frac{\tau}{\mu}}\left\{e^{-\frac{\delta}{\mu}}-e^{-\mathbf{A}\delta}\right\}\begin{bmatrix}\boldsymbol{\Psi_u}\\ \boldsymbol{\Psi_d}\end{bmatrix} \tag{A7}$$

On the other hand, we can also write the solution based on the interaction principle. For the scalar radiative transfer, reciprocity principle is valid which implies that reflection and transmittance matrices from the layer top are identical to that from the layer bottom. Therefore, upward radiation at the layer top is composed of transmitted upward radiation from the layer bottom, reflected downward radiation at the layer top, and upward layer source radiation from the layer top. Downward radiation at the layer bottom is composed of transmitted downward radiation from the layer top, reflected upward radiation at the layer bottom, and downward layer source radiation from the layer bottom. That is [58]:

$$\begin{bmatrix}I_u(0)\\ I_d(\delta)\end{bmatrix}=\begin{bmatrix}\boldsymbol{t} & r\\ r & \boldsymbol{t}\end{bmatrix}\begin{bmatrix}I_u(\delta)\\ I_d(0)\end{bmatrix}+\begin{bmatrix}\boldsymbol{S}_u\\ \boldsymbol{S}_d\end{bmatrix} \tag{A8}$$

Eq.(A8) can be rewritten (see Eq. (A7) of [13] as:

$$\begin{bmatrix}I_u(\delta)\\ I_d(\delta)\end{bmatrix}=\begin{bmatrix}\boldsymbol{t} & 0\\ -\boldsymbol{r} & \boldsymbol{E}\end{bmatrix}^{-1}\begin{bmatrix}\boldsymbol{E} & -r\\ 0 & \boldsymbol{t}\end{bmatrix}\begin{bmatrix}I_u(0)\\ I_d(0)\end{bmatrix}+\begin{bmatrix}\boldsymbol{t} & 0\\ -\boldsymbol{r} & \boldsymbol{E}\end{bmatrix}^{-1}\begin{bmatrix}-\boldsymbol{S}_u\\ \boldsymbol{S}_d\end{bmatrix} \tag{A9}$$

By comparing Eq.(A3) with Eq.(A9), we obtain

$$\begin{bmatrix}\boldsymbol{t} & 0\\ -\boldsymbol{r} & \boldsymbol{E}\end{bmatrix}^{-1}\begin{bmatrix}\boldsymbol{E} & -r\\ 0 & \boldsymbol{t}\end{bmatrix}=e^{-\mathbf{A}\delta} \tag{A10}$$

Or

$$e^{\mathbf{A}\delta} = \begin{bmatrix} \boldsymbol{E} & -\boldsymbol{r} \\ \boldsymbol{0} & \boldsymbol{t} \end{bmatrix}^{-1} \begin{bmatrix} \boldsymbol{t} & 0 \\ -\boldsymbol{r} & \boldsymbol{E} \end{bmatrix} = \begin{bmatrix} \boldsymbol{E} & \boldsymbol{r}\boldsymbol{t}^{-1} \\ \boldsymbol{0} & \boldsymbol{t}^{-1} \end{bmatrix} \begin{bmatrix} \boldsymbol{t} & 0 \\ -\boldsymbol{r} & \boldsymbol{E} \end{bmatrix} = \begin{bmatrix} \boldsymbol{t} - \boldsymbol{r}\boldsymbol{t}^{-1}\boldsymbol{r} & \boldsymbol{r}\boldsymbol{t}^{-1} \\ \boldsymbol{t}^{-1}\boldsymbol{r} & \boldsymbol{t}^{-1} \end{bmatrix} \tag{A11}$$

Eq.(A11) is the same as Eq.(2.14) of [59]. From Eq.(A11), we can obtain the analytic expression for the transmittance matrix (Eq.(8c)) and the reflection matrix [60]. By comparing source terms between Eq.(A7) and Eq.(A9), one can have

$$\begin{bmatrix} \boldsymbol{t} & 0 \\ -\boldsymbol{r} & \boldsymbol{E} \end{bmatrix}^{-1} \begin{bmatrix} -\boldsymbol{S}_u \\ \boldsymbol{S}_d \end{bmatrix} = b_1 \delta \begin{bmatrix} \boldsymbol{\Xi} \\ \boldsymbol{\Xi} \end{bmatrix} + \left\{ e^{-\mathbf{A}\delta} - \begin{bmatrix} \boldsymbol{E} & 0 \\ 0 & \boldsymbol{E} \end{bmatrix} \right\} \left\{ b_0 \begin{bmatrix} \boldsymbol{\Xi} \\ \boldsymbol{\Xi} \end{bmatrix} - \frac{1}{1-\omega g} b_1 \begin{bmatrix} -\boldsymbol{u}\boldsymbol{\Xi} \\ \boldsymbol{u}\boldsymbol{\Xi} \end{bmatrix} \right\} - e^{-\frac{\tau}{\mu}} \left\{ e^{-\frac{\delta}{\mu}} - e^{-\mathbf{A}\delta} \right\} \begin{bmatrix} \boldsymbol{\Psi}_u \\ \boldsymbol{\Psi}_d \end{bmatrix} \tag{A12}$$

Using Eq.(10) and rearranging terms in Eq.(A12), we can derive the analytic expression for layer source vectors in Eq.(8a) and Eq.(8b).

References

[1] Chandrasekhar S. Radiative Transfer. New York: Dover Publications Inc.; 1960.

[2] Lenoble J. Radiative transfer in scattering and absorbing atmospheres: standard computational procedures. A Deepak Publishing, 300p; 1985.

[3] Liou KN. An introduction to atmospheric radiation. Academic Press, New York, 392p; 1980.

[4] Hansen JE, Travis LD. Light scattering in planetary atmospheres. 1974, *Space Sci. Rev.* **16**, 527–610.

[5] de Haan JF, Bosma PB, Hovenier JW. The adding method for multiple scattering calculations of polarized light. *Astron. Astrophys.* 1987, **183**, 371–391.

[6] Hovenier JW, van der Mee C., Domke H. *Transfer of Polarized Light in Planetary Atmospheres—Basic Concepts and Practical Methods,* Kluwer Academic Publishers, Dordrecht, The Netherlands, 2004.

[7] Stamnes K., Radiative Transfer in the Atmosphere and Ocean, Cambridge University Press, 2017. https://doi.org/10.1017/9781316148549

[8] Fischer J, Grassl H. Radiative transfer in an atmospheric-ocean system: an azimuthally dependent matrix operator approach. *Appl. Opt.* 1984; **23**: 1032-1039.

[9] van de Hulst HC, A new look at multiple scattering, Goddard Institute for Space Studies, National Aeronautics and Space Administration, New York, NY, 1963.

[10] Evans KF. Stephens GL. A new polarized atmospheric radiative transfer model. *JQSRT*, 1991; **46**: 413-423.

[11] Spurr RJD, 2006: VLIDORT: A linearized pseudo-spherical vector discrete ordinate radiative transfer code for forward model and retrieved studies in multilayer multiple scattering media, *JQSRT*, 2006; **102**, 316-542.

[12] Ota Y., Higurashi A., Nakajima, Teruyuki T.,Yokota T., Matrix formulations of radiative transfer including the polarization effect in a coupled atmosphere–ocean system. *JQSRT*, 2010; **111**. 878-894. 10.1016/j.jqsrt.2009.11.021.

[13] Efremenko DSE, Garcia VM, Garcia SG, Doicu A. A review of the matrix-exponential formalism in radiative transfer. *JQSRT*, 2017, **196**: 17-45.

[14] Liou KN, Ou SC, Takano Y, Liu Q. A Polarized Delta-Four-Stream Approximation for Infrared and Microwave Radiative Transfer: Part I. *J. Atmos. Sci.* 2005; **62**:2542-2554.

[15] Heidinger, AK., O'Dell C., Bennartz R, Greenwald T. The successive order of interaction radiative transfer model, Part I: Model Development. *J. Applied Meteorol. Clim.* 2006; **45**, 1388-1402.

[16] Duan M, Min QL, Lu DR, A Polarized Radiative Transfer Model Based on Successive Order of Scattering, *Adv. in Atmos. Sci*.. 2010; **27**: 891-900.

[17] Voronovich AG, Gasiewski AJ, Weber BL. A fast multistream scattering-based jacobian for microwave radiance assimilation. *IEEE Geosci. Remote Sensing.,* 2004; **42**: 1749-1761.

[18] Weng F, Liu Q. Satellite Data Assimilation in Numerical Weather Prediction Models, Part I: Forward Radiative Transfer and Jocobian Modeling in Cloudy Atmospheres. *J. Atmos. Sci*., 2003; **60**:2633-2646.

[19] Liu Q, Weng F. Advanced Doubling-Adding Method for Radiative Transfer in Planetary Atmosphere, *J. Atmos. Sci.*, 2006; **63**: 3459–3465.

[20] Liu Q, Weng F. Using advanced matrix operator (AMOM) in community radiative transfer. 2013; IEEE JSTAR, 10.1109/JSTARS.2013.2247026.

[21] Hoffman, R, Louis J-F, Nehrkorn, T: A method for implementing adjoint calculations in the discrete case, Technical Memorandum, European Center for Medium-Range Weather Forecasts. *Miscellaneous Publisher*, 1992.

[22] Stephens GL. Remote Sensing of the Lower Atmosphere, An Introduction. Oxford University Press, 523p, 1994.

[23] Gehrels T. ed. Planets, Stars and Nebulae Studied with Photopolarimetry, University of Arizona Press, Tucson, AZ, 1974.

[24] Mishchenko MI, Rosenbush VK, Kiselev NN, *et al*. *Polarimetric Remote Sensing of Solar System Objects,* Akademperiodyka, Kyiv; 2010, http://arxiv.org/abs/1010.1171.

[25] Kolokolova L, Hough J, A.-C. Levasseur-Regourd A-C. Eds. *Polarimetry of Stars and Planetary Systems.* Cambridge University Press, Cambridge, 2015.

[26] Goodberlet M, Swift MCT, Wilkerson J. Ocean surface wind speed measurements of the Special Sensor Microwave/Imager (SSM/I). *IEEE Trans. Geosci. Remote Sensing*, 1990; **28**: 823-828.

[27] Wentz FJ. Measurement of the oceanic wind vector using satellite microwave radiometers, *IEEE Trans. Geosci. Remote Sens.,* 1992; **30**: 960-972.

[28] Miao, J, Johnsen KP, Kern S, Heygster G, K. Kunzi K. Signature of Clouds over Antarctic Sea Ice Detected by the Special Sensor Microwave/Imager. *IEEE Trans. Geosci. Remote Sensing*, 2000; **38**: 2333-2344.

[29] Chepfer, H, Goloub P, Riedi J, De Haan JF, Hovenier JW, Flamant PH. Ice crystal shapes in cirrus clouds derived from POLDER/ADEOS-1. *J. Geophys. Res.*, 2000; **106**: 7955-7966.

[30] Weinman JA, Guetter PJ. Determination of rainfall distributions from microwave radiation measured by the Nimbus 6 ESMR, *J. Appl. Meteorol*., 1977; **16**: 437-442.

[31] Liu Q, Ruprecht E. A radiative transfer model: matrix operator method. *Appli. Opt.*, 1996; **35**: 4229-4237.

[32] Chen Y, Han Y, Weng F. Comparison of two transmittance algorithms in the community radiative transfer model: Application to AVHRR, *J. Geophys. Res*., 2012; **117**, D06206, doi:10.1029/2011JD016656.

[33] Mishchenko MI, Travis LD, Lacis AA. Multiple Scattering of Light by Particles: Radiative Transfer and Coherent Backscattering, Cambridge University Press, Cambridge, UK, 2006.

[34] Lacis, A. A., J. Chowdhary, M. I. Mishchenko, and B. Cairns, Modeling errors in diffuse-sky radiation: vector vs. scalar treatment. *Geophys. Res. Lett. 1998,* **25**, 135–138.

[35] Mishchenko MI, Travis LD, Lacis AA. *Scattering, Absorption, and Emission of Light by Small Particles* Cambridge University Press, Cambridge, UK, 2002.

[36] Stamnes K, Tsay S-C, Wiscombe W, Jayaweera K. Numerically stable algorithm for discrete ordinate method radiative transfer in multiple scattering and emitting layered media. *Appli Opt.* 1988; **27**:2502–9.

[37] Anderson E, Bai Z, Bischof C, Demmel J, Dongarra J, Du Croz J, et al. LAPACK user's guide, 2nd Ed. Philadephia: *Society for Industrial and Applied Mathematics*; 1995.

[38] Liu Q, Lu S. Community Radiative Transfer Model for Air Quality Studies (chapter 2), Light Scattering Reviews, Volume 11, pp 67-115, Springer Praxis Books, Springer-Verlag, Berlin – Heidelberg, 2016.

[39] Selby JEA, Clough SA. User Guide to LOWTRAN 7. AFGL-TR-88-0177 Geophysics Directorate/GPOS, Hanscom AFB, 1988.

[40] Siewert CE. A discrete-ordinates solution for radiative transfer models that include polarization effects. *JQSRT* 2000; **64**:227–54.

[41] Schulz FM, Stamnes K. Angular distribution of the Stokes vector in a plane-parallel vertically inhomogeneous medium in the vector discrete ordinate radiative transfer (VDISORT) model. *JQSRT* 2000; **65**:609–20.

[42] Mishchenko, MI. Electromagnetic Scattering by Particles and Particle Groups: An Introduction, Cambridge University Press, Cambridge, UK, 2014.

[43] Yueh S., Kwok R., Nghiem SV., Polarimetric scattering and emission properties of targets with reflection symmetry, 1994, **29**, 1409-1420.

[44] Aronson R., Radiative transfer implies a modified reciprocity relation. J. Opt. Soc. Am. A, 1997; **14**, 486-490.

[45] Girolamo LD., Reciprocity principle for radiative transfer models that use periodic boundary conditions, *JQSRT*, 2002; **73**, 23-27.

[46] Fung T. Computation of the matrix exponential and its derivatives by scaling and squaring, Int. *J. Numer. Meth. Engng* 2004; **59**:1273–1286 (DOI: 10.1002/nme.909)

[47] Mackowski, DW. A general superposition solution for electromagnetic scattering by multiple scattering domains of optically active media. *J. Quant. Spectrosc. Radiat. Transfer 2014,* **133**, 264–270.

[48] Mackowski DW, Mishchenko MI. A multiple sphere *T*-matrix Fortran code for use on parallel computer clusters. *J. Quant. Spectrosc. Radiat. Transfer* 2011, **112**, 2182–2192.

[49] Kahnert M. The T-matrix code *Tsym* for homogeneous dielectric particles with finite symmetries. *J. Quant. Spectrosc. Radiat. Transfer. 2013,* **123**, 62–78.

[50] Bi L, Yang P, Kattawar GW, Mishchenko MI. Efficient implementation of the invariant imbedding T-matrix method and the separation of variables method applied to large nonspherical inhomogeneous particles. *J. Quant. Spectrosc. Radiat. Transfer. 2013,* **116**, 169–183.

[51] Mishchenko MI, Geogdzhayev IV, Yang P. Expansion of tabulated scattering matrices in generalized spherical functions. *J. Quant. Spectrosc. Radiat. Transfer. 2016,* **183**, 78–84.

[52] Wauben WMF, Hovenier JW. Polarized radiation of an atmosphere containing randomly-oriented spheroids. *JQSRT* 1992; ***47***:491–504

[53] Liu Q, Weng F. Combined Henyey-Greenstein and Rayleigh (HG-Rayleigh) Phase Function, *Appl Opt*, 2006; **45**, 7475-7479.

[54] Yang P, Liou KN, Mishchenko MI, Gao BC. Efficient finite-difference time-domain scheme for light scattering by dielectric particles: application to aerosols. *Appl Opt*, 2000; **39**: 3727-3737.

[55] Mishchenko M, Hovenier J, Travis L, editors. Light scattering by non-spherical particles. Newyork: Academic Press; 2000.

[56] Coulson K, Dave J, Sekera D. Tables related to radiation emerging from planetary atmosphere with Rayleigh scattering. Berkeley:University of California Press; 1960.

[57] Haferman JL, Krajewski WF, Smith TF, Sanchez A. Radiative transfer for a three-dimensional raining cloud. *Appl. Opt*., 1993; **32**: 2795-2802.

[58] Liu Q. A radiative budget index at the top of the atmosphere derived from METEOSAT climate data set. Report of Institut fuer Meereskunde, University of Kiel, Nr 216; 1991.

[59] Waterman PC. Matrix-exponential description of radiative transfer. *J Opt Soc Am* 1981;**71**:410-422.

[60] Liu Q. An analytical solution of transmission and reflection operators for homogeneous atmospheres. *Contri. Atmosph. Phys.*, 1990; **63**, 128-133.

Figure Caption

Figure 1. An interface diagram of the Community Radiative Transfer Model. The modules in the public interfaces (upper dashed box) are accessed by users. The modules in the bottom dashed box are for developers.

Figure 2. Comparisons of the phase function (a), linear polarization of the phase function (b) using the original (black line), HG-Rayleigh (blue line), Rayleigh (yellow line), and Henyey-Greenstein phase functions (red line). There is no polarization in the HG.

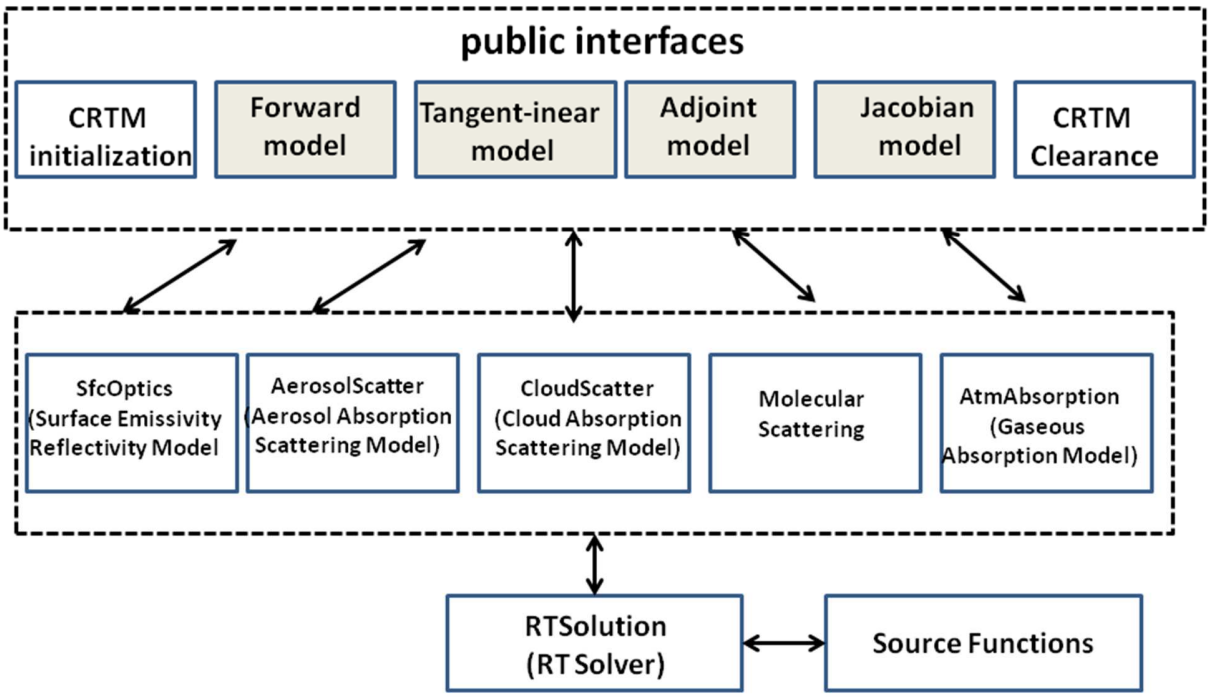

Figure 1. An interface diagram of the Community Radiative Transfer Model. The modules in the public interfaces (upper dashed box) are accessed by users. The modules in the bottom dashed box are for developers.

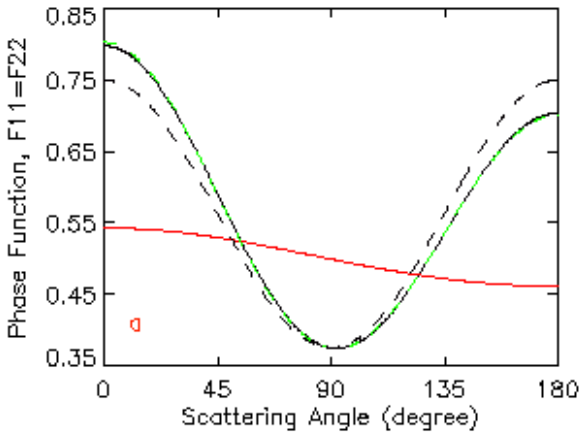
0.85
0.75
0.65
0.55
0.45
0.35
Phase Function, F11=F22
a
0
45
90
135
180
Scattering Angle (degree)

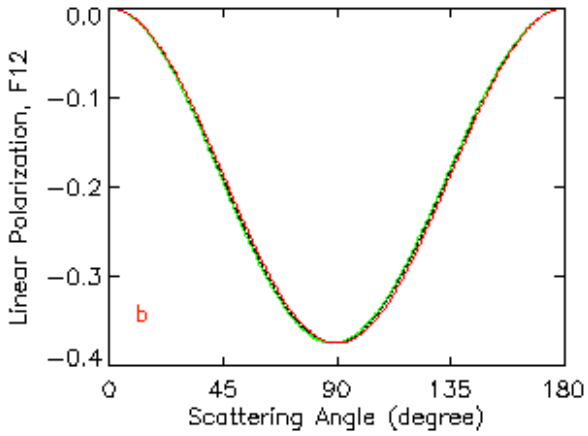
0.0
−0.1
−0.2
−0.3
−0.4
Linear Polarization, F12
b
0
45
90
135
180
Scattering Angle (degree)

Figure 2. Comparisons of the phase function (a), linear polarization of the phase function (b) using the original (black line), HG-Rayleigh (green line), Rayleigh (black dashed line), and Henyey-Greenstein phase functions (red line). There is no polarization in the HG.

Table 1a. Legendre expansion coefficients for Rayleigh scattering.

	F_{11}	F_{22}	F_{33}	F_{44}	F_{12}	F_{43}
0	1.0	1.0	0.0	0.0	-0.5	0.0
1	0.0	0.0	1.5	1.5	0.0	0.0
2	0.5	0.5	0.0	0.0	0.5	0.0

Table 1b. Greek matrix coefficients for Rayleigh scattering

	F_{11}	F_{22}	F_{33}	F_{44}	F_{12}	F_{43}
0	1.0	0.0	0.0	0.0	0.0	0.0
1	0.0	0.0	0.0	1.5	0.0	0.0
2	0.5	3.0	0.0	0.0	$\sqrt{6}/2$	0.0

Table 2a. . Legendre expansion coefficients for an atmosphere of randomly oriented oblate spheroids.

	F_{11}	F_{22}	F_{33}	F_{44}	F_{12}	F_{43}
0	1.0	0.0	0.929287	0.0	0.967924	0.915207
1	2.104031	0.0	2.118711	0.0	2.073916	2.095727
2	2.095158	-0.116688	3.615946	0.065456	3.726079	2.008624
3	1.414939	-0.209370	2.240516	0.221658	2.208680	1.436545
4	0.703593	-0.227137	1.139473	0.097752	1.190694	0.706244
5	0.235001	-0.144524	0.365605	0.052458	0.391203	0.238475
6	0.064039	-0.052640	0.082779	0.009239	0.105556	0.056448
7	0.012837	-0.012400	0.013649	0.001411	0.020484	0.009703
8	0.002010	-0.002093	0.001721	0.000133	0.003097	0.001267
9	0.000246	-0.000267	0.000172	0.000011	0.000366	0.000130
10	0.000024	-0.000027	0.000014	0.000001	0.000035	0.000011
11	0.000002	-0.000002	0.000001	0.0	0.000003	0.000001

Table 2b. Greek matrix coefficients for an atmosphere of randomly oriented oblate spheroids

	F_{11}	F_{22}	F_{33}	F_{44}	F_{12}	F_{43}
0	1.0	0.0	0.0	0.915267	0.0	0.0
1	2.104031	0.0	0.0	0.095727	0.0	0.0
2	2.095158	3.726079	3.615946	2.008624	-0.116688	0.065456
3	1.414939	2.202868	2.240516	1.436545	-0.209370	0.221658
4	0.703593	1.190694	1.139473	0.706244	-0.227137	0.097752
5	0.235001	0.391203	0.365605	0.238475	-0.144524	0.052458
6	0.064039	0.105556	0.082779	0.056448	-0.052640	0.009239
7	0.012837	0.020484	0.013649	0.009703	-0.012400	0.001411
8	0.002010	0.003097	0.001721	0.001267	-0.002093	0.000133
9	0.000246	0.000366	0.000172	0.000130	-0.000267	0.000011
10	0.000024	0.000035	0.000014	0.000011	-0.000027	0.000001
11	0.000002	0.000003	0.000001	0.000001	-0.000002	0.0

Table 3a. . Legendre expansion coefficients for HG-Rayleigh phase matrix.

	F_{11}	F_{22}	F_{33}	F_{44}	F_{12}	F_{43}
0	1.0	1.000101	0.041291	0.041291	-0.499556	-0.000064
1	0.081467	0.081467	1.500544	1.500544	-0.013013	0.000000
2	0.500993	0.500993	0.053196	0.053196	0.499411	0.000064
3	0.013024	0.013024	0.000695	0.000695	0.013011	-0.000000

Table 3b. . Greek matrix coefficients for HG-Rayleigh phase matrix.

	F_{11}	F_{22}	F_{33}	F_{44}	F_{12}	F_{43}
0	1.0	0.0	0.0	0.0	0.0	0.041291
1	0.081467	0.0	0.0	0.0	0.0	1.500544
2	0.500993	-1.223599	0.145575	0.000156	3.000788	0.053196
3	0.013024	-0.023758	0.001271	-0.000000	0.043401	0.000695

Table 4a. Pure Rayleigh atmosphere of optical depth of 0.1 using 4 streams (2 in upward and 2 in downward direction). The solar flux is normalized to π, the solar zenith angle is 36.8699 (the cosine of the solar zenith angle is 0.8), and the surface albedo is 0.25. Single scattering albedo is 1.0. VLIDORT requires the single scattering is less than 1.0 and we use the single scattering albedo of 0.99999. The upwelling radiance is for a viewing (zenith) angle of 50.21 degree.

	I	Q	U	V
DA	0.215409	-0.000316	-0.020898	0.0
VLIDORT	0.215409	-0.000316	-0.020898	0.0
ADA	0.215409	-0.000316	-0.020897	0.0
AMOM	0.215409	-0.000316	-0.020897	0.0

Table 4b. Same as Table 4a, but using 16 streams

	I	Q	U	V
DA	0.216527	-0.000214	-0.021456	0.0
VLIDORT	0.216526	-0.000214	-0.021456	0.0
ADA	0.216526	-0.000214	-0.021455	0.0

AMOM	0.216526	-0.000214	-0.021455	0.0

Table 5a. Same as Table 4a, but for an optical depth of 1.

	I	Q	U	V
DA	0.374199	0.008465	-0.124870	0.0
VLIDORT	0.374189	0.008464	-0.124868	0.0
ADA	0.374197	0.008467	-0.124864	0.0
AMOM	0.374196	0.008467	-0.124864	0.0

Table 5b. Same as Table 5a, but using 16 streams

	I	Q	U	V
DA	0.372577	0.007767	-0.124787	0.0
VLIDORT	0.372567	0.007767	-0.124785	0.0
ADA	0.372575	0.007770	-0.124782	0.0
AMOM	0.372574	0.007770	-0.124781	0.0
Coulson et al. (1960)	0.37248	-0.00774	0.12476	0.0

Table 6. Same as Table 4b (16 streams), but using the phase function for an atmosphere of randomly oriented oblate spheroids.

	I	Q	U	V
DA	0.200216	0.000149	-0.000396	0.000001
VLIDORT	0.200215	0.000149	-0.000396	0.000001
ADA	0.200216	0.000149	-0.000396	0.000001
AMOM	0.200216	0.000149	-0.000396	0.000001

Table 7. Same as Table 6, but for an optical depth of 1.

	I	Q	U	V
DA	0.247890	0.001246	-0.007078	0.000019
VLIDORT	0.247882	0.001246	-0.007078	0.000019
ADA	0.247888	0.001246	-0.007077	0.000019
AMOM	0.247888	0.001246	-0.007077	0.000019

Table 8. Same as Table 6, but for an optical depth of 10.

	I	Q	U	V
DA	0.557838	0.003928	-0.012050	0.000044
VLIDORT	0.557727	0.003927	-0.012050	0.000044
ADA	0.557839	0.003928	-0.012050	0.000044
AMOM	0.557828	0.003928	-0.012050	0.000044

Table 9. Same as Table 6, but for an optical depth of 100.

	I	Q	U	V
DA	0.761506	0.003850	-0.012050	0.000044
VLIDORT	0.760356	0.003850	-0.012050	0.000044
ADA	0.761511	0.003850	-0.012050	0.000044
AMOM	0.761395	0.003850	-0.012050	0.000044

Table 10. Comparison of CPU time usage between VLIDORT and AMOM. Phase function for an atmosphere of randomly oriented oblate spheroids and 16 streams are used. The solar flux is normalized to π, the solar zenith angle is 36.8699 (the cosine of the solar zenith angle is 0.8), and the surface albedo is 0.25. Single scattering albedo is 1.0. VLIDORT requires the single scattering is less than 1.0 and we use the single scattering albedo of 0.99999. The upwelling radiance is for a viewing (zenith) angle of 50.21 degree.

Layer optical depth	VLIDORT (seconds)	AMOM (seconds)
100	0.096	0.076
10	0.096	0.063
1	0.096	0.054
0.1	0.095	0.048